Assessing the complementarity of future hybrid wind and solar photovoltaic energy resources for North America

X. Costoya [a,*], M. deCastro [a], D. Carvalho [b], M. Gómez-Gesteira [a]

[a] Centro de Investigación Mariña, Universidade de Vigo, Environmental Physics Laboratory (EPhysLab), Campus da Auga, 32004, Ourense, Spain
[b] CESAM, Physics Department, University of Aveiro, 3810-193, Aveiro, Portugal

ARTICLE INFO

ABSTRACT

Renewable energy plays a key role into achieving the international targets for reducing global greenhouse gas emissions. Considering that these forms of energy are dependent on climate conditions and that their variability occurs at different time scales, it is important to analyze the complementarity to ensure a stable power supply to the grid in the context of climate change. A multi-model ensemble of 10 global climate models from the CMIP6 project was used to analyze the complementarity between wind and solar photovoltaic power in North America from 2025 to 2054 under the SSP2-4.5 scenario. This complementarity was evaluated using two indices that account for the similarity between the two resources (Similarity index, S_i) and the temporal complementarity (Concurrency index, C_i). The combination of the two resources reduced spatial heterogeneity in terms of annual mean power in North America. The highest values of S_i were detected west of California and in the Caribbean Sea, and the lowest were found in Mexico. Regarding C_i, the highest values were detected in ocean areas north of 30°N. Both indices were divided into four categories to assess the most suitable areas for combining wind and solar photovoltaic power. Coastal areas in the Gulf of Mexico and substantial areas in the Caribbean Sea are considered optimal in terms of complementarity. Inland, good complementarity was observed on the US-Canada border (e.g., the Great Lakes) and in northern areas such as Alaska or the Labrador Peninsula. The lowest values of complementarity were detected in Mexico.

1. Introduction

The development of renewable energy systems is paramount to reduce greenhouse gases emissions to achieve international decarbonization targets (e.g., the Paris Agreement [1]). Therefore, the transition from conventional fossil energy sources to clean renewable energy plays a key role in climate change mitigation [2]. However, although renewable energy sources are crucial to mitigate climate change, they are also dependent on weather conditions, which are expected to change in a global warming context [3]. It is estimated that global efforts to increase the use of clean renewable energy resources will increase the share of electricity generation by these sources from the estimated 25% in 2017 to roughly 85% in 2050 [4].

Globally, solar PV and wind capacity have experienced rapid growth in recent years: solar PV saw an increase of 162 GW in 2022 (50% higher than in 2019), whereas global wind capacity increased by more than 90% in 2020 [5]. This global increase was also reflected in North America: regarding wind energy, this region was the second most

prominent worldwide, with the highest annual new installed capacity in 2020 and the third highest in 2021, accounting for 14% of new wind installations, behind Asia Pacific (59%) and Europe (19%) [6]. In addition, the United States had the second highest new wind power capacity of any country in 2021 with 13.01 new GW installed, which was surpassed only by China. Considering total wind power capacity, Canada occupies the ninth position in the world [7]. Regarding solar PV power, North America had an installed solar PV capacity of ~104 GW in 2021, with the US accounting for ~90% (93.7 GW) followed by Mexico with ~7 GW and Canada with 3.6 GW [8]. Currently, Asia and Europe have higher solar PV installed capacity than North America, however, it is expected that North America will have the second-highest installed solar PV capacity (~430 GW) by 2030 [9]. Therefore, North America is a region where an important development of wind and solar PV power is expected. This observation is in accordance with the various Nationally Determined Contributions (NDCs) presented by the countries of North America under the Paris Agreement. In this context, Canada has recently updated its commitment to reduce greenhouse gasses emissions by 40–45% below 2005 levels by 2030 [10]. As for the US, the commitment

Nomenclature

CBO	Congressional Budget Office
CMIP	coupled model intercomparison project
CORDEX	coordinated regional climate downscalling experiment
C_I	concurrency index
ECMWF	european centre for medium-range weather forecasts
ERA	ECMWF atmospheric reanalysis
GCMs	global climate models
GDP	Gross Domestic Product
hPa	hectopascal
IPCC	intergovernmental panel on climate change
NDC	Nationally Determined Contribution
OP	overlap percentage
PDF	Probability density function
PV	Photovoltaic
PVres	Photovoltaic solar power resource
PDF	Probability density function
RCMs	regional climate models
RSDS	shortwave downward radiation
SSP	shared socioeconomic pathway
S_I	similarity index
UNFCCC	United Nations Framework Convention on Climate Change
W	Watts
WPD	wind power density

achieved is to reduce its net greenhouse gas emission by 50–52% in 2030 compared to 2005 [11]. These targets should be achieved in a context of population growth in North America over the upcoming decades. According to the United Nations [12] population growth of ~12% is expected in 2050 compared to 2022. In addition, an increase in the main macroeconomic parameters, such as Gross Domestic Product (GDP), is also forecast [13,14]. In this way, commitments to reduce fossil fuel dependency in conjunction with population growth and economic shifts highlight the need to develop new ways to exploit renewable energies in the near future.

Climate models are one of the most used tools to analyze the impact of climate change on renewable energies. Phase 6 of the Coupled Model Intercomparison Project (CMIP6) represents the state of the art of climate projection [15]. CMIP6 encompasses various simulations carried out with Global Climate Models (GCMs) that make climate projections based on different Shared Socioeconomic Pathways (SSPs) [16]. SSPs are scenarios that represent different socio-economic developments with different assumptions about education, urbanization, economic growth, greenhouse gases, aerosol emissions, energy supply and demand, land-use changes, and other factors [17]. SSPs differ from other parameters in their stabilized radiative forcing, or in other words, the difference between the incoming energy from the Sun and the energy radiated into space. Recently, different studies have used data from the CMIP6 project to analyze the impact of climate change on wind and solar PV power. Carvalho et al. [18] analyzed wind energy projections in Europe during the 21st century under SSP2-4.5 and SSP5-8.5, whereas Martinez & Iglesias [19] carried out a similar analysis in North America. Data from the GCMs of the CMIP6 project were also used to carry out future wind resource variations at regional scale. Akinsola et al. [20] analyzed changes in wind energy potential over West Africa. Qian & Zhang [21] studied future changes in the wind energy resource over the Northwest Passage, and Zhang & Li [22] analyzed future offshore wind energy resource variation in China. Also related to future wind energy changes, Moradian et al. [23] studied variations in wind speed in the United Kingdom and Deng et al. [24] analyzed variations in this variable over China using an ensemble of GCMs. As for the analysis of future variations in solar photovoltaic power using data from the CMIP6 simulations, Dutta et al. [25] carried out a global analysis of projected changes in solar energy potential using a multi-model ensemble and considering three SSPs. Hou et al. [26] used a multi-model ensemble to analyze future variations of solar PV power in Europe.

To date, projections of wind and solar PV power carried out with GCMs from the CMIP6 project have focused on analyzing renewable resources individually, without considering their combination. Given that renewable sources will be predominant in future electricity generation, it is also important to analyze the spatial and temporal complementarity between different renewable energy resources to ensure a stable power supply to the grid. Each renewable energy has its own inherent production variability that depends on local climate characteristics. Therefore, a hybrid system using different renewable resources that are complementary can improve the reliability of energy generation. In addition, co-location of different renewable resources can lead to benefits regarding infrastructure and land usage, which may reduce economic costs. Acknowledging this, a combined climate impact analysis can clarify whether energy stability will be minimized or augmented [27]. For this reason, there is increasing interest in analyzing future combined projections of renewable energy power. In this context, various combined analyses have been carried out with data from previous phases of the CMIP project (e.g. Ref. [28]). In addition, numerous studies (e.g. Refs. [29–32]) have been carried out using future climate projections derived from older CMIP generations (e.g., CMIP5, CMIP3) and/or their respective downscaling initiatives such as CORDEX, EN-SEMBLES, etc. The complementarity of different renewable resources can be analyzed with different metrics and indices (detailed information about these methodologies can be found in Ref. [33]).

This study aimed to analyze the effect of climate change on wind and solar photovoltaic power in North America using the latest future climate projections from the CMIP6 project, which served as a basis for the latest IPCC 6th Assessment Report (REF). The analysis focused on the coming decades because a rapid increase was expected in the exploitation of both renewable resources in this region over this period. The analysis will be carried out in terms of the mean production of each resource, which will be then integrated into a combined analysis to estimate the impact of climate change on the temporal stability of the combined production. To the authors' knowledge, this is the first study to analyze the complementarity between wind and solar PV power in terms of energy supply stability using CMIP6 data. In addition, new indices were created to evaluate this complementarity. The methodology, as well as the data used to carry out the study, are described in Section 2. Results are shown in Section 3 and discussed in Section 4. The main conclusions of the study are presented in Section 5.

2. Data and methods

2.1. Data

Historical and projected wind-power density (WPD) and solar photovoltaic (PV) power were analyzed using simulations from the sixth phase of the Coupled Model Intercomparison Project (CMIP6) [15]. To analyze PV power, three variables are necessary: surface downwelling shortwave radiation, temperature measured at 2 m above sea level, and wind speed measured at 10 m above sea level. This last variable is the only one necessary to calculate WPD. Data were downloaded from the Earth System Grid Federation (ESGF) data portal: https://esgf-data.dkrz.de/search/cmip6-dkrz/.

The CMIP6 project offers data from multiple GCMs. The existence of the three atmospheric variables at a daily temporal resolution and with a horizontal spatial resolution of at least $1.25° \times 1.25°$ (latitude $\times$

longitude) was the criterion used to select the GCM simulations. A total of 10 GCM simulations fulfilled these conditions and were selected to carry out the analysis (Table 1). The Shared Socioeconomic Pathway (SSP) selected was SSP2-4.5, which is a middle-of-the-road scenario that assumes that greenhouse gas emissions will increase until 2050 and then steadily decline until 2100.

Analyzing more in detail the expected evolution of the global-average carbon dioxide (CO_2), methane (CH_4), and nitrous oxide (N_2O) in greater detail revealed, it is expected that the CO_2 concentration of CO_2 will be around 506 ppm in 2050 and 602.8 ppm in 2100 [34]. CH_4 will increase until 2050 (2020 ppb) and then will decrease until 2100 (1683 ppb), whereas N_2O is expected to slight increase slightly throughout the 21st Century under this scenario (343 ppb in 2050 and 354 ppb in 2100). This evolution in greenhouse gasses concentrations can be translated into a radiative forcing of 4.5 W/m2 at the end of the century, which will cause a temperature increase of 2.5 °C when compared to the pre-industrial era. The SSP2-4.5 scenario does not consider significant trend variations regarding social, economic, and technological aspects compared to historical patterns. It assumes a moderate increase in the global population, with a peak of 9.4 billion people around 2070 and a stabilization in the second half of the century [35]. Regarding energy demand, an increase is expected reaching values of 640 EJ/y by 2050 and 970 EJ/y by 2100 [36]. From an environmental point of view, a degradation is also expected because a slow progress in achieving sustainable development objectives by global and national institutions is assumed. Finally, this scenario also includes the assumption that the income inequality will persist or improve only slowly.

The present analysis has also considered the SSP5-8.5 scenario, which is a business-as-usual scenario that assumes that greenhouse gas emissions will not be sufficiently limited, and that radiative forcing will reach 8.5 W/m^2 in 2100 [16]. This scenario projects rapid growth of the global economy based on high global energy demand. This choice was made because the lack of coordinated and well-founded policies worldwide to reduce greenhouse gas emission [37] could drive to this scenario. In this way, a scenario based on development along historical patterns (SSP2-4.5) and another one based on development driven by extensive fossil-fuel use (SSP5-8.5) were selected. Results from the SSP5-8.5 scenario will be presented only in the Appendix.

A multi-model ensemble approach based on calculating the various parameters for each GCM, and then averaging the results to produce a global value was followed. Previous analyses ([38,39]) have shown that this approach reduces the biases and uncertainties of individual models. Because each GCM has its own spatial resolution, it was necessary to remap all GCMs to a common spatial grid. Hence, the 10 GCMs were remapped to a common spatial grid with a resolution of 1° × 1.25° (latitude × longitude). Regarding the period analyzed, a historical period (1985–2014) and a near-future period (2025–2054) were considered. Two periods of 30 years were chosen because this is the minimum time span that should be considered to analyze climate change [40]. The complementarity between the two resources was analyzed for 2025–2054 because a rapid increase in both renewable resources is expected during the coming decades, with the aim of achieving global greenhouse gas emissions reduction targets in the region. The historical period was considered to assess model quality by comparing numerical results with the ERA5 reanalysis; the future period was used to calculate future projections of energy resources.

Table 1
Global climate models from the CMIP6 project [15] used in this study.

GCM	Institute	GCM	Institute
MPI-ESM1-2-HR	MPI-M	NorESM2-MM	NCC
TaiESM1	AS-REC	MRI-ESM2-0	MRI
CMCC-CM2-SR5	CMCC	CESM2-WACCM	NCAR
CMCC-ESM2	CMCC	CM4	GFDL
EC-Earth3	EC-Earth	ESM4	GFDL

The reliability of CMIP6 GCMs to represent WPD and solar PV contemporary climatologies was evaluated by comparing them with data from the ERA5 reanalysis [41], which is the latest state-of-the-art reanalysis from the European Centre for Medium-Range Weather Forecasts. Previous studies have already used the ERA5 dataset to validate data from CMIP6 GCMs. (e.g: [18]). ERA5 data were retrieved from the Copernicus Climate Data Store Service (https://cds.climate.copernicus.eu/cdsapp#!/dataset/reanalysis-era5-single-levels?tab=form). The spatial horizontal resolution of ERA5 is 0.25° × 0.25°. Hourly data for the three variables used in the present analysis are available from 1979 onwards. To carry out the comparison with CMIP6 GCMs simulations, ERA5 data were daily averaged and re-gridded to the same common grid as the CMIP6 GCMs.

2.2. Methods

2.2.1. Wind power density and solar photovoltaic power calculation

The photovoltaic solar power resource (PV_{res}) was calculated following the methodology developed by Jerez et al. [42]. This calculation is mainly based on the use of the shortwave downward radiation that the earth's surface receives from the Sun. However, it also considers a correction for the negative effect that an increase in temperature has on PV cell efficiency [43]. This method is based on the following expression:

$$PV_{res} = P_R * RSDS \tag{1}$$

where $RSDS$ refers to the shortwave downward radiation (Wm^{-2}) and P_R is a performance ratio that accounts for the effect of temperature on PV cell efficiency. Detailed information on the P_R calculation can be found in Jerez et al. [42] or Costoya et al. [44].

On the other hand, WPD was calculated as:

$$WPD = \frac{1}{2}\rho_a W_H^3 \tag{2}$$

where ρ_a is the air density (1.225 kgm^{-3} at 288.15 K and 1000 hPa) and W_H is the wind speed at the selected hub height (100 m). The WPD metric is widely used in wind energy studies because it only considers the wind energetic resource available in the atmosphere. Hence, it facilitates comparison among different areas to analyze the most favorable zones for wind turbines installations.

WPD was calculated at 100 m because the typical hub height of wind turbines has increased significantly in the past few decades [45]. In addition, it is expected to increase even more during the next decades. The typical hub height of offshore wind turbines is even higher nowadays [46]. Therefore, the selected height to extrapolate WPD values represents a good balance between land-based and offshore wind turbines and also considers the future development of this technology. To carry out the extrapolation from 10 m to 100 m the following expression was used:

$$W_H = W_{ns} \left(\frac{H}{H_{ns}}\right)^\alpha \tag{3}$$

where H is the selected height to extrapolate winds (100 m a.g.l/a.s.l); H_{ns} is the height at which near-surface winds are measured; W_{ns} is the wind speed measured at H_{ns}; W_H is the wind speed at the desired measurement height H and α is an empirically derived coefficient that varies according to atmospheric stability. A common value for this exponent used in wind resource assessment is 1/7 (neutrally stable atmosphere) for land areas ([47,48]). However, a lower value is more suitable over water [48]. Considering that the present analysis encompasses land and ocean areas the approach developed by Carvalho et al. [18], was followed. These authors analyzed future WPD changes in Europe by means of CMIP6 GCMs. Using ERA5 wind speed data at 10 m and 100 m, they calculated the α exponent that best fit land areas and ocean waters. They obtained a value of 0.17 for land areas and 0.06 for water bodies.

PV_{res} and WPD were calculated for each grid point and each GCM from the CMIP6 project. After that, following the multi-model approach, values from each GCM were averaged for each grid point.

2.2.2. CMIP6 GCM validation

The reliability of CMIP6 GCMs to reproduce WPD and $PVres$ values was evaluated by comparing them with values from the ERA5 reanalysis. This comparison was carried out for the historical period (1985–2014). The metric used to carry out the validation process was the overlapping percentage (OP). Its calculation was based on a study by Perkins et al. [49]. It has been previously used in several renewable energy analyses (e.g. Refs. [18,50,51]). The OP metric is based calculating the probability density functions (PDFs) for each series. The minimum value between the ERA5 and GCM series was then selected for each bin and finally all the minima were summed. This process can be mathematically summarized in the following expression:

$$OP = \sum_{i=1}^{n} minimum\left(Z_i^m, Z_i^{ERA}\right) * 100 \tag{4}$$

where n is the number of bins used to calculate the PDFs of each variable (WPD or PV_{res}), and Z_i^{ERA} and Z_i^m are the frequencies of values of the ERA5 and the GCM simulation respectively for each bin i. Therefore, an OP value of 100 means a perfect match between the ERA5 and the simulated data. This metric was calculated for each of the ten GCMs from CMIP6. In this way, the reliability of each GCM could be known, and the calculation of both renewable resources could be reproduced. In addition, this approach also makes it possible to determine the performance of the multi-model ensemble in reproducing the variables analyzed. This procedure was applied for each grid point of the area under study.

2.2.3. Indices for evaluating the complementarity between WPD and PV_{res}

Different metrics were implemented to assess the complementarity between wind and PV solar energy resources to accurately design hybrid solutions in North America. Briefly, two new indices based on analysis of the similarity and temporal complementarity of WPD and PV_{res} were implemented. Detailed information regarding these metrics is given below.

2.2.3.1. Similarity index.

This index evaluates the degree of similarity of WPD and PV solar power in terms of averaged power throughout the period analyzed. Taking advantage of the fact that both series are measured in Wm^{-2}, an index to analyze the degree of similarity in power intensity at annual scale was developed:

$$S_I^{i,j} = \frac{min\left(WPD^{i,j}, PV_{res}^{i,j}\right)}{max\left(WPD^{i,j}, PV_{res}^{i,j}\right)} \tag{5}$$

where the superscripts i and j correspond to the grid points, WPD and PV_{res} are the annual power resources (in Wm^{-2}), and min and max represent the minimum and the maximum values between the two resources calculated for every grid point. A value close to one is obtained when WPD and PV_{res} are very similar, which is desirable, whereas the more different the intensity of the two resources, the lower S_I will be. The similarity index was calculated for every CMIP6 model.

2.2.3.2. Concurrency index.

A concurrency index (C_I) was created to analyze the temporal simultaneity between both resources for each grid point (i,j) according the expression:

$$C_I^{i,j} = \frac{1 - \rho^{i,j}}{2} \tag{6}$$

where $\rho^{i,j}$ is the correlation between $WPD^{i,j}$ and $PV_{res}^{i,j}$ calculated as:

$$\rho^{i,j} = \frac{Cov\left(WPD^{i,j}, PV_{res}^{i,j}\right)}{\sigma\left(WPD^{i,j}\right)\sigma\left(PV_{res}^{i,j}\right)} \tag{7}$$

where Cov is the covariance and σ the standard deviation.

It is important to bear in mind that to provide an efficient supply of energy to the grid based on renewable energies, it is necessary that the renewable energies balance each other throughout the year. Hence, according to C_I, the most desirable situation (value of 1) is obtained when both resources are perfectly anti-correlated. The concurrency index was calculated for every CMIP6 model.

2.2.3.3. Combined index.

With the aim of discovering the locations that best suit the complementarity between both energy resources, both indices (S_I and C_I) were first classified into four categories (Table 2) and then blended into a combined index.

3. Results

3.1. Capability of CMIP6 simulations to reproduce WPD and PV_{res} data

The 10 simulations of the CMIP6 project (Table 1) were validated by comparing them with ERA5 reanalysis. As explained in Section 2.2.2, the validation was done in terms of OP because this metric can compare the whole data distribution. OP was applied over the WPD and PV_{res} values for each grid point over the historical period, 1985–2014. This approach made it possible to validate the whole study area. Fig. 1 shows OP for WPD and solar PV_{res} in North America. Regarding OP for WPD (Fig. 1a), values over 70% were obtained for WPD in most of North America. In addition, higher values (>85%) were obtained over the ocean, whereas lower values were detected over land, with values ranging from 70% to 80%. It is well-known that land areas have more complex topography than ocean surfaces and that this fact causes higher inaccuracies and biases when wind speed is simulated onshore. Regarding OP for PV_{res} (Fig. 1b), values higher than 80% were obtained throughout the area under study, and north of 30° latitude, values were higher than 90%.

To determine whether there are differences in the representation of WPD and solar PV_{res} among the ten GCMs used to construct the multi-model ensemble, a global OP value was calculated for each GCM (Table 3). The global OP value was calculated by averaging the OP values of all the grid points in the study area. Overall, high OP values (>80%, with the exception of one GCM for WPD) were obtained both for solar PV_{res} and WPD. Because the differences between GCMs were slight, the ten GCMs available were considered suitable to construct the multi-model ensemble. In addition, the global average OP for all GCMs was 90.5% for PV_{res} and 84.0% for WPD. Carvalho et al. [18] compared wind speeds from different CMIP6 models with ERA data by means of OP in Europe. Although it is important to remember that the analyzed variable and the region under study are different, the values obtained in the present analysis are slightly higher than those obtained by these authors. In addition, the OP values from Table 3 are similar to OP values obtained in other studies that analyzed renewable energies in the United States (e. g. Ref. [52]). Therefore, it can be concluded that the 10 GCMs from the CMIP6 project can properly represent WPD and solar PV_{res} in North America and that the CMIP6 multi-model ensemble is an appropriate

Table 2
Classification category of S_I and C_I.

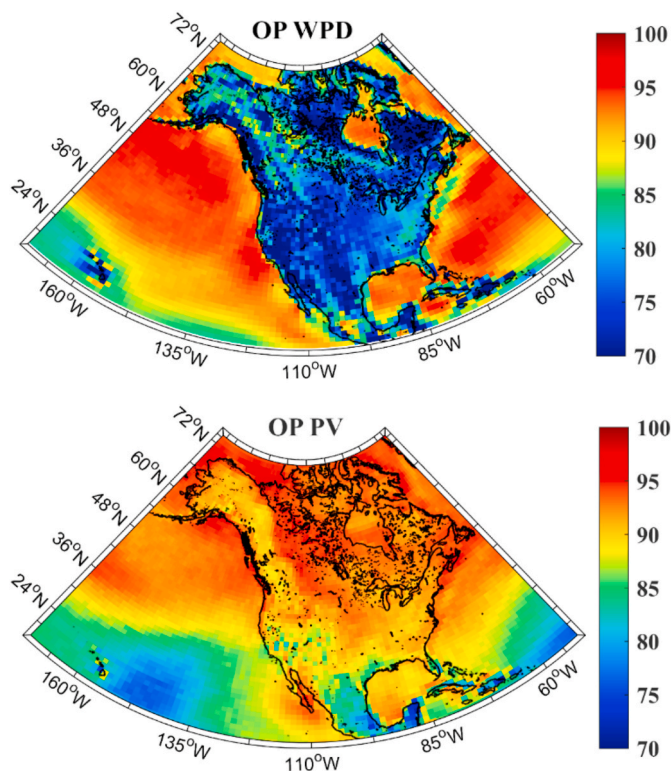|		Categorization value	
Category	Degree of complementarity	S_I	C_I
1	Poor	x < 0.25	x < 0.25
2	Marginal	0.25 ≤ x ≤ 0.50	0.25 ≤ x ≤ 0.50
3	Good	0.50 ≤ x ≤ 0.75	0.50 ≤ x ≤ 0.75
4	Optimal	x > 0.75	x > 0.75

Fig. 1. Overlap percentage (OP, %) between the multi-model ensemble of CMIP6 simulations and ERA5 dataset for the wind power density (*WPD*) and the solar photovoltaic power.

Table 3
Overlap percentage between each GCM and ERA5 database for North America over the period 1985–2014.

GCM	OP (%)	
	PV_{res}	*WPD*
CESM2-WACCM	89.4	86.3
CMCC-CM2-SR5	91.0	82.8
CMCC-ESM2	90.8	82.5
EC-Earth3	93.2	88.3
GFDL-CM4	90.7	85.8
GFDL-ESM4	90.1	82.7
MPI-ESM1-2-HR	89.2	85.0
MRI-ESM2-0	91.0	79.2
NorESM2-MM	89.0	86.2
TaiESM1	90.4	81.5
GCM average	**90.5 ± 1.2**	**84.0 ± 2.8**

tool to carry out the present study.

3.2. Mean values of future wind and solar power resources

The annual mean PV_{res} in North America for the near future is shown in Fig. 2a. A clear latitudinal gradient is apparent, as expected, with lower values (~100 W m^{-2}) in the northernmost zone of North America and higher values (~250 W m^{-2}) in the southern part (Mexico and oceanic areas south of 24°N). Fig. 2b shows the annual mean *WPD*. Different patterns between land and ocean were detected. It is well known that *WPD* over land is lower than over ocean because of the greater roughness of land due to complex topography and the presence of many natural obstacles that reduce wind speed. Hence, annual mean *WPD* values lower than 300 W m^{-2} were found over land, with the highest values in the innermost part of the continent. However, values higher than 300 W m^{-2} were detected in most of the oceanic parts of North America. The highest values (~1000 W m^{-2}) were observed north of 36°N, whereas values around 500 W m^{-2} prevailed in the oceanic regions south of this latitude, except for the western coast of Mexico, where lower values were observed. Similar annual patterns of the mean solar photovoltaic power and the wind power density were obtained under the SSP5-8.5 scenario (Figure A1).

Finally, the combined resource ($WPD + PV_{res}$) was also represented with the aim of assessing the potential viability of using both renewable resources in the same location (Fig. 3). In annual average terms, a more homogeneous pattern was obtained compared with the PV_{res} power pattern (Fig. 2a) or the *WPD* one (Fig. 2b), with the exception of the ocean north of 36°N, where values higher than 1000 W m^{-2} were found due to the high *WPD* resource observed in these areas. Over land, combined values ranged from 250 to 500 W m^{-2}, with the highest values in the innermost area of the continent. A similar annual pattern of the combined resource ($WPD + PV_{res}$) was obtained under the SSP5-8.5
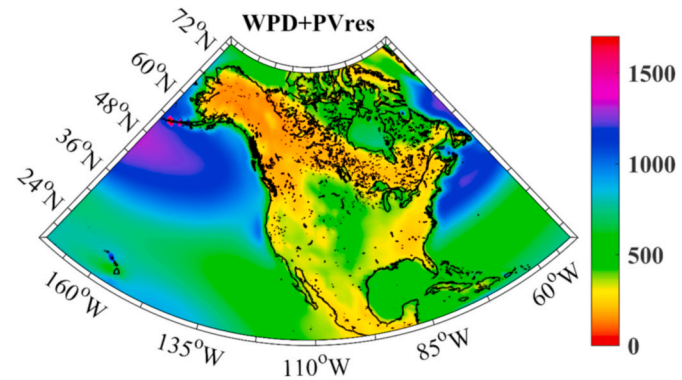

Fig. 3. Annual mean $WPD + PV_{res}$ (Wm^{-2}) calculated by means of the CMIP6 multi-model ensemble in North America over the near future (2025–2054) under the SSP2-4.5 scenario.
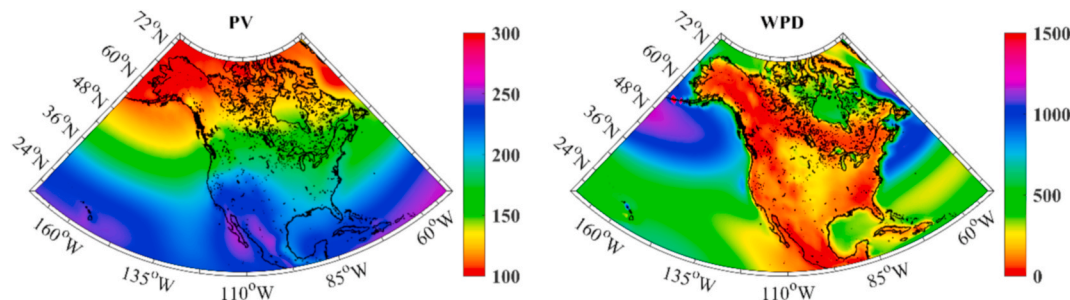

Fig. 2. Annual mean (a) solar photovoltaic power (Wm^{-2}) and (b) wind power density calculated by means of the CMIP6 multi-model ensemble in North America over the near future (2025–2054) under the SSP2-4.5 scenario.

scenario (Figure A2).

3.3. Analysis of the complementarity between WPD and PV_res power

S_I, which represents the degree of similarity between WPD and PV_{res} in terms of mean power, is shown in Fig. 4. High S_I values (>0.7) were found in the ocean south of 24°N, especially along the Gulf of Mexico, in the Caribbean Sea, and in the ocean area around the California Peninsula. This fact is related to the high PV_{res} power detected in the southernmost zone (Fig. 2a) and the high WPD over the ocean compared to over land (Fig. 2b). In fact, the lowest S_I values were detected in some areas of Mexico because the PV_{res} power is high, but the WPD is low over these continental areas. As for the S_I values for land areas in Canada and USA, values higher than 0.6 were detected in most of these areas, although lower values were observed in the western part of the continent.

An analysis of the temporal complementarity of the two resources was carried out in terms of the Concurrency Index (Fig. 5). Values higher than 0.6 were obtained in most of North America except for the western coast around the California Peninsula and some areas of Mexico, such as the Yucatan Peninsula or the northeastern corner, where lower values (<0.5) were observed. The highest values were detected in the Pacific Ocean north of 24°N. Similar patterns for the similarity and concurrence indices were obtained under the SSP5-8.5 scenario (Figure A3 and A.4).

S_I (similarity between resources) and C_I (temporal complementarity) were categorized into four classes (Fig. 6). According to Table 2, Class 1 means the worst possible value from the point of view of resource stability, whereas Class 4 is the best (optimal). Regarding S_I (Fig. 6a), the highest values (Class 4) were obtained in marine areas of the Gulf of Mexico, Caribbean Sea, and the western area of the California Peninsula. Over the continent, higher values (Class 3) were detected in the innermost area of North America than in areas near the coastline, although some coastal areas such as Alaska or the northeastern coast were also categorized as Class 3. Regarding the classification according to the concurrency index (Fig. 6b), most of the study area was classified in Class 3. However, important areas such as the Hawaiian Islands and most of Mexico were categorized as Class 2 (marginal). Similar results were also obtained under the SSP5-8.5 scenario (Figure A5).

Finally, the areas with the best features in terms of complementarity between wind and solar PV power were mapped (Fig. 7). An area was considered to present good complementarity when it was classified as *good* on both the S_I and C_I indices. In addition, an area that was considered optimal for one index and at least good for the other was classified as *optimal*. In this way, most of the coastal area of the Gulf of Mexico, as well as important areas of the Caribbean Sea such as Cuba, were classified as optimal in terms of complementarity between the two resources. In addition, an oceanic area south of 24°N and around 115°W
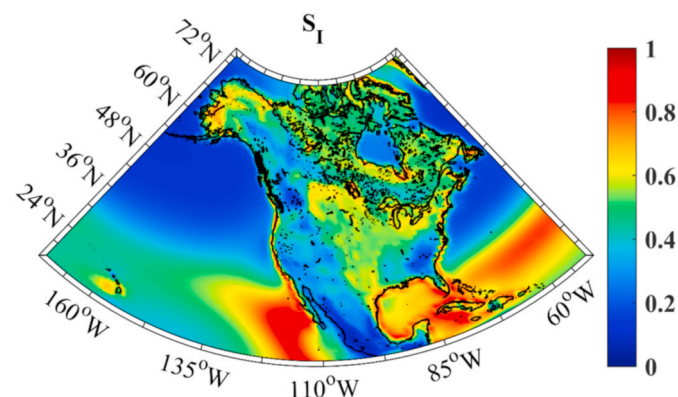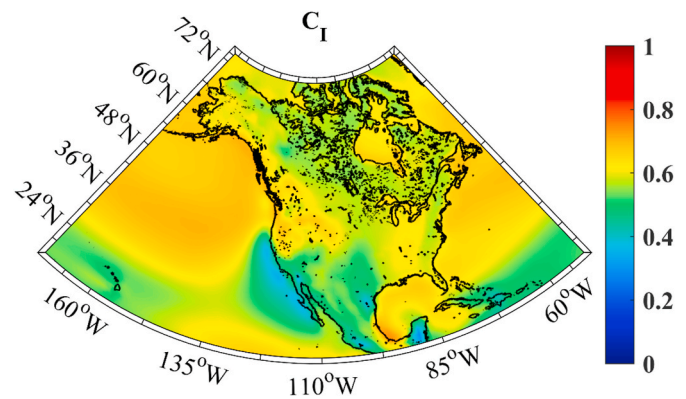

Fig. 5. Concurrency index (C_I) calculated by means of the CMIP6 multi-model ensemble in North America over the near future (2025–2054) under the SSP2-4.5 scenario.

was also considered optimal. This area classified as optimal will be higher under the SSP5-8.5 scenario (Figure A6). In terrestrial North America, good complementarity was found in the inner continent, especially along the border between the United States and Canada, in areas such as the Great Lakes. Furthermore, vast areas of Alaska and the Labrador Peninsula were also classified as good. Regarding ocean areas, most of the Gulf of Mexico, the Caribbean Sea, and the Atlantic Ocean south of 24°N were classified as good.

4. Discussion

Spatial differences in mean future solar photovoltaic power (Fig. 2a) and wind-power density (Fig. 2b) were observed in North America over the near future by means of a multi-model ensemble of 10 GCMs from the CMIP6 project. The spatial heterogeneity observed in PV_{res} and WPD when analyzed individually is attenuated when both resources are combined (Fig. 3). This occurs mainly because low WPD values over the continent (orange color in Fig. 2a) are compensated for by higher PV_{res} values. In addition, the highest WPD occurred in oceanic areas north of 36°N, where the lowest values of PV_{res} were also found.

Previous studies analyzed both solar PV power and WPD projections at specific locations in North America with simulations carried out with various regional climate models (RCMs). Haupt et al. [53] analyzed both resources for the contiguous United States, and Losada-Carreño et al. [30] used a RCM to downscale 5 GCMs from CMIP5 to analyze the impact of climate change on wind and solar PV power in Texas. However, these studies analyzed wind and solar PV separately without considering their spatial and temporal complementarity. Therefore, to the authors' knowledge, the present study represents the first attempt to assess the complementarity between the two renewable resources in North America considering the effect of climate change and taking advantage of a CMIP6 multi-model ensemble. In the only similar study, Jerez et al. [29] studied combined wind and solar PV power production and its correlation by means of a CORDEX (CMIP5 downscaling) multi-model ensemble, but in Europe.

The classification of the new indices (S_I, Fig. 4 and C_I, Fig. 5) into four categories (Fig. 6) provides an integrated and comprehensive view of the future complementarity between WPD and PV_{res} by distinguishing the areas where the combined resource will be good or optimal (Fig. 7). When focusing on nearshore areas, the highest complementarities are obtained in the Gulf of Mexico and some Caribbean countries, such as Cuba or the Bahamas, which are classified as optimal. This is an interesting fact because islands are often isolated energy systems where offshore renewable sources can represent a great opportunity. New technological solutions for offshore wind energy such as floating platforms and offshore PV solar energy ([54] can anticipate an important development over the coming years. In fact, various studies (e.g. Refs.
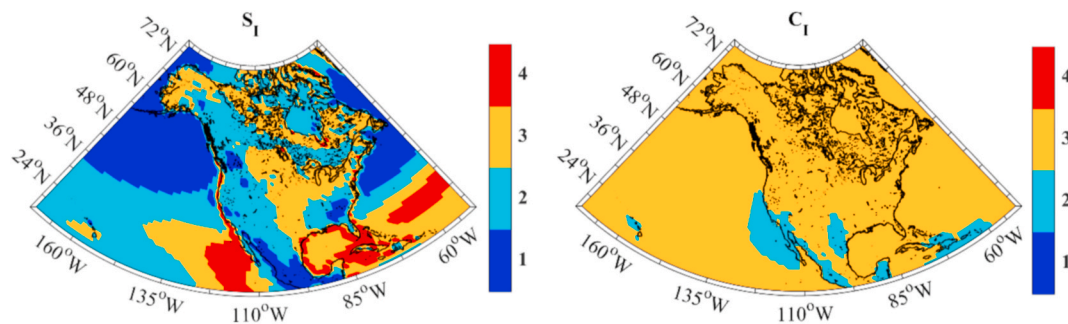

Fig. 4. Similarity index (S_I) calculated by means of the CMIP6 multi-model ensemble in North America over the near future (2025–2054) under the SSP2-4.5 scenario.

Fig. 6. (a) Similarity index (S$_I$) and (b) Concurrency index (C$_I$) range classification in North America from the CMIP6 multi-model ensemble over the near future (2025–2054).
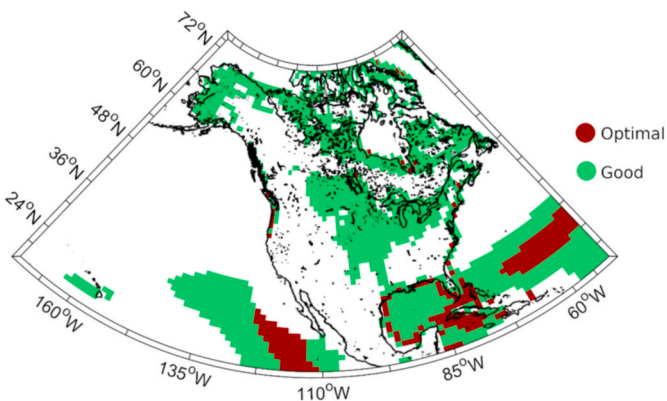

Fig. 7. Most suitable areas for combining wind and solar photovoltaic power.

[44,55]) have already analyzed the benefits of combining offshore wind and solar PV energy for other areas of the globe. Therefore, considering the high degree of complementarity in the Gulf of Mexico and the Caribbean Sea, this can be a viable energy alternative for these regions. In terms of land areas, a high degree of complementarity was obtained in the innermost part of North America, which was rated as good, especially along the border between the United States and Canada, for example in the Great Lakes. In addition to Alaska, some areas of Hawaii and the oceanic area west of Mexico were also classified as good. Finally, the lowest complementarity values were detected in Mexico (Fig. 6). This was related to the low *WPD* (Fig. 2b) and the high solar PV power values (Fig. 2a) detected in this area. In addition, both resources showed low concurrency (blue color in Fig. 6b).

The results previously described provide information that can help policymakers adopt and modify strategies to improve the stability of the energy supply. In addition, they could be useful for evaluating the number of wind turbines or PV solar panels that optimize the stability considering the average mean power production of each type of energy (Fig. 2; Fig. 3). Although the present analysis of complementarity between wind and solar PV power was carried out with a multi-model of the most recent climate change projections, future analysis should be carried out considering two other important aspects: On the one hand, a similar analysis to that provided in the present manuscript should be done at hourly temporal resolution because both renewable resources have strong intra-daily variations, especially solar PV power. On the other hand, it is important to consider the specific energy demand of each area where wind and solar PV power are combined, because the ultimate goal is to better adjust the supply-demand balance through renewable energies. For these purposes, it is necessary to carry out simulations with RCM for each specific location. Furthermore, technological developments such as improvements in energy storage systems will help to achieve this goal [56].

Besides the benefits regarding the balance of the energy supply to the grid, it is important to mention that hybrid solar-wind systems could present other advantages. From an infrastructure point of view, only a single grid connection point is necessary and land is used more efficiently. These aspects could favor a lower Levelized Cost of Electricity ([57,58]). For these reasons, various hybrid power plants involving solar PV and wind have been developed in recent years, including pilot projects and even larger plants (e.g., Haringvliet Hybrid Energy Park in The Netherlands) [58]. One of these pilot projects has been developed in Minnesota (USA). Therefore, important growth in solar-wind hybrid energy systems utilizations can be expected in coming decades. However, it is worth noting that environmental, political, and economic issues should be considered in such energy developments. The regulatory and legal aspects of importance depend on each country [59]. Regarding technical issues, aspects such as sizing of hybrid systems (e.g. Ref. [57]) or different system structures [60] (Roy et al., 2022) are being analyzed. In addition, wind turbines and solar PV panels are also expected to become more efficient in the upcoming decades. For this reason, the present analysis focused on the *WPD* and *PV$_{res}$* resources, and no specific wind turbine or solar PV panel model was selected. From an economic point of view, the macroeconomic implications of decarbonization scenarios are multiple (employment, GDP, welfare, debt, etc) [61]. A positive or negative impact on these fields will be conditioned by structural changes in energy supply and demand systems. At this level, hybrid solar-wind systems can favor a more efficient transition that reduces the economic impacts of decarbonization policies.

5. Concluding remarks

The effect of climate change on the complementarity between wind and solar photovoltaic power was assessed in North America for the near future (2025–2054) under the CMIP6 SSP2-4.5 and SSP5-8.5 future climate scenarios. The analysis was carried out using a CMIP6 multi-model ensemble that had been previously validated with the ERA5 reanalysis. Two new indices were implemented to provide a more integrated and comprehensive view of the complementarity between *WPD* and *PV$_{res}$*. The similarity in terms of intensity between both renewable resources (S$_I$) and their temporal concurrency (C$_I$) was explored. These indices were then classified and integrated in a combined index to assess the locations that best suit the complementarity between the two energy resources. The main findings of this study can be summarized as follows:

- A high degree of similarity (S$_I$) between the two renewable resources was detected in the Gulf of Mexico, the Caribbean Sea, the coastal fringe of the southern Pacific Ocean, and in most of the inner continent of North America.
- A high temporal concurrency (C$_I$) was obtained in most of North America except for the coastal fringe around California and some areas of Mexico, Hawaii and the eastern Caribbean Sea.
- The degree of complementarity between *PV$_{res}$* and *WPD* was estimated as optimal in the coastal zone of the Gulf of Mexico, some

zones of the Caribbean Sea, and in the oceanic zone west of Mexico. In addition, it was considered good inland along the US-Canada border (e.g., the Great Lakes) and in northern areas such as Alaska or the Labrador Peninsula. The lowest complementarities were detected in Mexico.

This study represents the first attempt to analyze the future complementarity between the two most important renewable energy sources in North America in the context of climate change. This information is relevant for improving the stability of the energy supply because substantial development of renewable energy sources is expected, with the aim of achieving international decarbonization targets. However, this research represents only a first step; future analyses at finer spatial and temporal resolution are necessary to combine both resources at specific locations and ensure energy supply-demand balance.

Author statement

Xurxo Costoya: Conceptualization, Methodology, Software, Writing - Original Draft, Writing – Review & Editing, Data curation, Formal Analysis. Maite deCastro: Data curation, Software, Methodology, Resources, Formal Analysis. David Carvalho: Writing - Review & Editing, Investigation, Formal Analysis, Data curation. **Moncho Gómez-Gesteira**: Software, Supervision, Visualization.

Declaration of competing interest

The authors declare that they have no known competing financial interests or personal relationships that could have appeared to influence the work reported in this paper.

Data availability

Data will be made available on request.
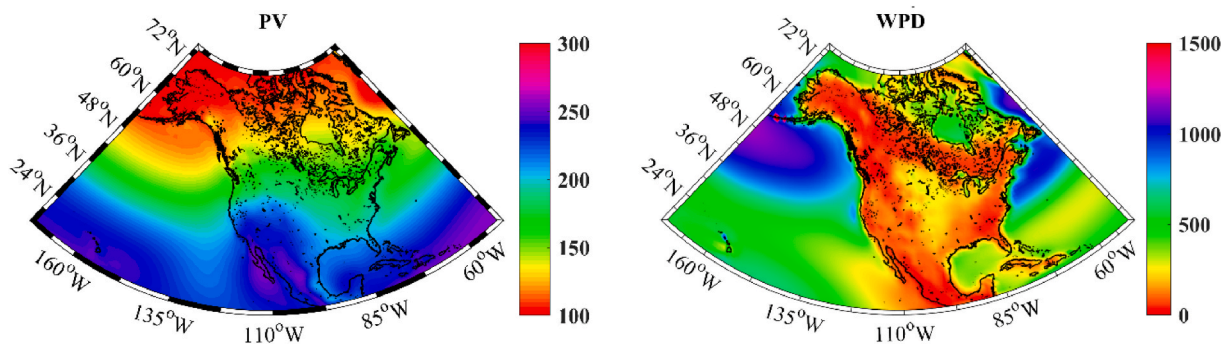
APPENDIX

Fig. A.1. Annual mean (a) solar photovoltaic power (Wm^{-2}) and (b) wind power density calculated by means of the CMIP6 multi-model ensemble in North America over the near future (2025–2054) under the SSP5-8.5 scenario.
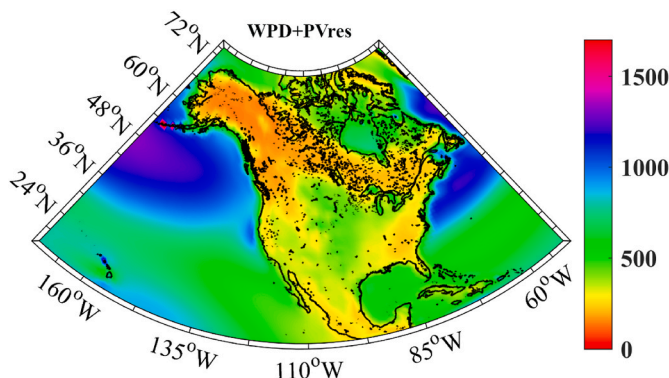
Fig. A.2. Annual mean $WPD + PV_{res}$ (Wm^{-2}) calculated by means of the CMIP6 multi-model ensemble in North America over the near future (2025–2054) under the SSP5-8.5 scenario.
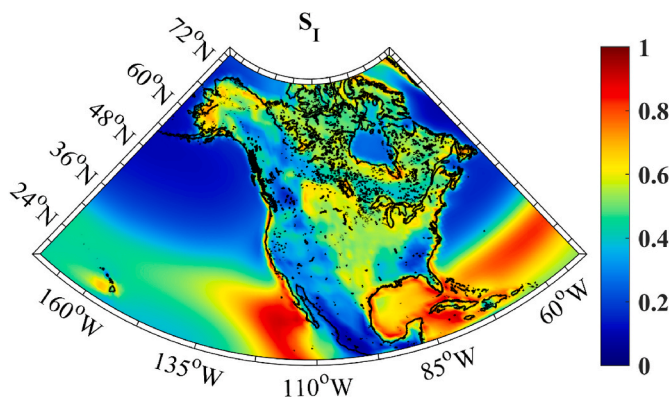

Fig. A.3. Similarity index (S$_I$) calculated by means of the CMIP6 multi-model ensemble in North America over the near future (2025–2054) under the SSP5-8.5 scenario.
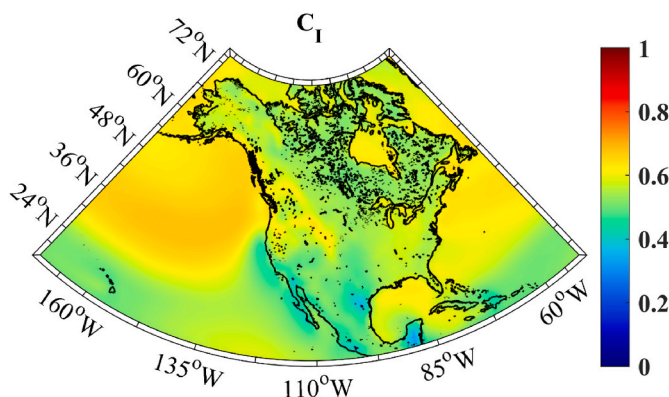

Fig. A.4. Concurrency index (C$_I$) calculated by means of the CMIP6 multi-model ensemble in North America over the near future (2025–2054) under the SSP5-8.5 scenario.
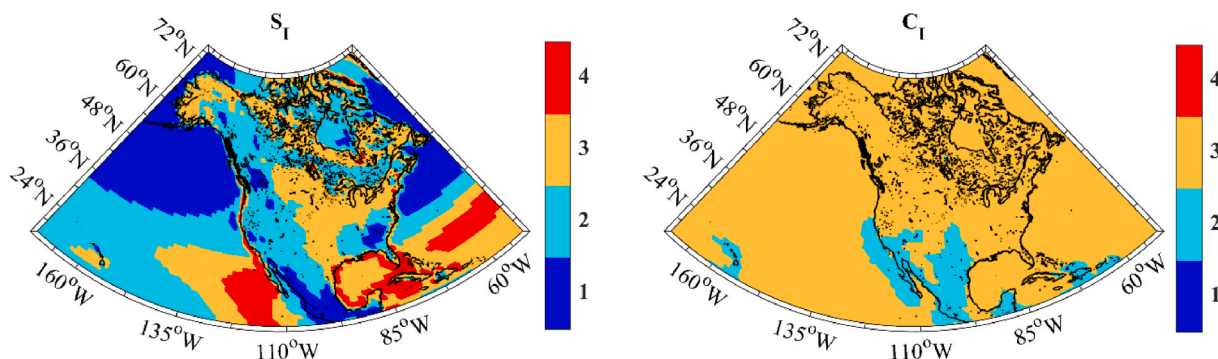

Fig. A.5. (a) Similarity index (S$_I$) and (b) Concurrency index (C$_I$) range classification in North America from the CMIP6 multi-model ensemble over the near future (2025–2054).
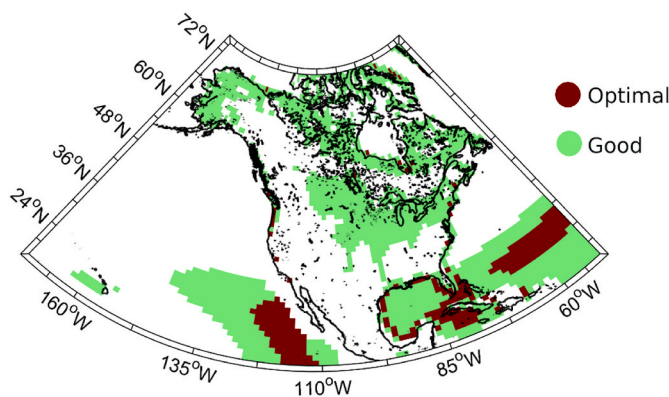

Fig. A.6. Most suitable areas for combining wind and solar photovoltaic power.

References

[1] Falkner R. The Paris Agreement and the new logic of international climate politics. Int Aff 2016;92(5):1107–25.

[2] IPCC. Climate Change. Mitigation of climate change. Contribution of working group III to the sixth assessment Report of the intergovernmental panel on climate change. In: Shukla PR, Skea J, Slade R, Al Khourdajie A, van Diemen R, McCollum D, Pathak M, Some S, Vyas P, Fradera R, Belkacemi M, Hasija A, Lisboa G, Luz S, Malley J, editors. Cambridge university press; 2022. NY, USA: Cambridge, UK and New York; 2022. https://doi.org/10.1017/9781009157926.

[3] Solaun K, Cerdá E. Climate change impacts on renewable energy generation. A review of quantitative projections. Renew Sustain Energy Rev 2019;116:109415.

[4] IRENA, International Renewable Energy Agency. Global energy transformation: a roadmap to 2050 (2019 edition). 2019. Abu Dhabi. Available at:.

[5] IEA, International Energy Agency. Renewable energy market update. 2021. Available online.

[6] GWEC, Global Wind Energy Council. Global wind report 2022. 2022. Available at:.

[7] CanREA. Canadian renewable energy association. 2022. Available at:.

[8] IRENA, International Renewable Energy Agency. Renewable capacity statistics. 2022. 2022. Abu Dhabi. Available at:.

[9] IRENA, International. Renewable Energy Agency. Future of Solar Photovoltaic: deployment, investment, technology, grid integration and socio-economic aspects. 2019. Abu Dhabi. Available at:.

[10] UNFCC, United Nations Framework Convention on Climate Change. Canada's 2021 nationally determined contribution under the Paris Agreement. 2021. Available at:.

[11] UNFCC, United Nations Framework Convention on Climate Change. The United States of America nationally determined contribution. Available at. 2021.

[12] United Nations. Department of economic and social affairs. Population Division 2022. World Population Prospects 2022, Online Edition. Available at:.

[13] Hawksworth J, Clarry R, Audino H. How will the global economic order change by 2050. Price water house Coopers (PWC), UK 2017. Available at:.

[14] CBO, Congressional Budget Office. 2022. CBO's. Report the 2022 long-term Budget outlook. 2022. Available at:.

[15] Eyring V, Bony S, Meehl GA, Senior CA, Stevens B, Stouffer RJ, Taylor KE. Overview of the coupled model intercomparison project phase 6 (CMIP6) experimental design and organization. Geosci Model Dev (GMD) 2016;9:1937–58.

[16] O'Neill BC, Tebaldi C, Van Vuuren DP, Eyring V, Friedlingstein P, Hurtt G, & Sanderson BM. The scenario model intercomparison project (ScenarioMIP) for CMIP6. Geosci Model Dev. 2016 2016;9(9):3461–82. https://doi.org/10.5194/gmd-9-3461-2016.

[17] Riahi K, Van Vuuren DP, Kriegler E, Edmonds J, O'neill BC, Fujimori S& Tavoni M. The shared socioeconomic pathways and their energy, land use, and greenhouse gas emissions implications: an overview. Global Environ Change 2017;42:153–68.

[18] Carvalho D, Rocha A, Costoya X, DeCastro M, Gómez-Gesteira M. Wind energy resource over Europe under CMIP6 future climate projections: what changes from CMIP5 to CMIP6. Renew Sustain Energy Rev 2021;151:111594.

[19] Martinez A, Iglesias G. Climate change impacts on wind energy resources in North America based on the CMIP6 projections. Sci Total Environ 2022;806:150580.

[20] Akinsanola AA, Ogunjobi KO, Abolude AT, Salack S. Projected changes in wind speed and wind energy potential over West Africa in CMIP6 models. Environ Res Lett 2021;(4):16. 044033.

[21] Qian H, Zhang R. Future changes in wind energy resource over the Northwest Passage based on the CMIP6 climate projections. Int J Energy Res 2021;45(1):920–37.

[22] Zhang S, Li X. Future projections of offshore wind energy resources in China using CMIP6 simulations and a deep learning-based downscaling method. Energy 2021;217:119321.

[23] Moradian S, Akbari M, Iglesias G. Optimized hybrid ensemble technique for CMIP6 wind data projections under different climate-change scenarios. Case study: United Kingdom. Sci Total Environ 2022;826:154124.

[24] Deng H, HuaW, Fan G. Evaluation and projection of near-SurfaceWind speed over China based on CMIP6 models. Atmosphere 2021;1062:12. https://doi.org/10.3390/atmos12081062.

[25] Dutta R, Chanda K, Maity R. Future of solar energy potential in a changing climate across the world: a CMIP6 multi-model ensemble analysis. Renew Energy 2022;188:819–29.

[26] Hou X, Wild M, Folini D, Kazadzis S, Wohland J. Climate change impacts on solar power generation and its spatial variability in Europe based on CMIP6. Earth Syst Dyn 2021;12(4):1099–113.

[27] Cronin J, Anandarajah G, Dessens O. Climate change impacts on the energy system: a review of trends and gaps. Clim Change 2018;151(2):79–93.

[28] Fant C, Adam Schlosser C, Strzepek K. The impact of climate change on wind and solar resources in southern Africa. Appl Energy 2016;161:556–64. https://doi.org/10.1016/j.apenergy.2015.03.042.

[29] Jerez S, Tobin I, Turco M, Jiménez-Guerrero P, Vautard R, Montávez JP. Future changes, or lack thereof, in the temporal variability of the combined wind-plus-solar power production in Europe. Renew Energy 2019;139:251–60.

[30] Losada Carreño I, Craig MT, Rossol M, Ashfaq M, Batibeniz F, Haupt SE, Brancucci C. Potential impacts of climate change on wind and solar electricity generation in Texas. Clim Change 2020;163(2):745–66.

[31] Fortes P, Simoes SG, Amorim F, Siggini G, Sessa V, Saint-Drenan YM, Assoumou E. How sensitive is a carbon-neutral power sector to climate change? The interplay between hydro, solar and wind for Portugal. Energy 2022;239:122106.

[32] Wang S, Zhu J, Huang G, Baetz B, Cheng G, Zeng X, Wang X. Assessment of climate change impacts on energy capacity planning in Ontario, Canada using high-resolution regional climate model. J Clean Prod 2020;274:123026.

[33] Jurasz J, Canales FA, Kies A, Guezgouz M, Beluco A. A review on the complementarity of renewable energy sources: concept, metrics, application and future research directions. Sol Energy 2020;195:703–24.

[34] Meinshausen M, Nicholls ZR, Lewis J, Gidden MJ, Vogel E, Freund M & Wang RH. 2020. The shared socio-economic pathway (SSP) greenhouse gas concentrations and their extensions to 2500. Geosci Model Dev (GMD) 2020;13(8):3571–605.

[35] Kc S, Lutz W. The human core of the shared socioeconomic pathways: population scenarios by age, sex and level of education for all countries to 2100. Global Environ Change 2017;42:181–92.

[36] Fricko O, Havlik P, Rogelj J, Klimont Z, Gusti M, Johnson N,& Riahi K. The marker quantification of the Shared Socioeconomic Pathway 2: a middle-of-the-road scenario for the 21st century. Global Environ Change 2017;42:251–67.

[37] Smith MR, Myers SS. Impact of anthropogenic CO_2 emissions on global human nutrition. Nat Clim Change 2018;8(9):834–9.

[38] Pierce DW, Barnett TP, Santer BD, Gleckler PJ. Selecting global climate models for regional climate change studies. Proc Natl Acad Sci. 2009 2009;106(21):8441–6.

[39] Jacob D, Petersen J, Eggert B, Alias A, Christensen OB, Bouwer LM. Yiou P. EURO-CORDEX: new high-resolution climate change projections for European impact research. Reg Environ Change 2014;14(2):563–78.

[40] WMO, World. Meteorological Organization. WMO guidelines on the calculation of climate normals. 2017. Available at:.

[41] Hersbach H, Bell B, Berrisford P, Hirahara S, Horányi A, Muñoz-Sabater J, Thépaut JN. The ERA5 global reanalysis. Q J R Meteorol Soc 2020;146(730):1999–2049.

[42] Jerez S, Tobin I, Vautard R, Montávez JP, López-Romero JM, Thais F, Wild M. The impact of climate change on photovoltaic power generation in Europe. Nat Commun 2015;6(1):1–8.

[43] Radziemska E. The effect of temperature on the power drop in crystalline silicon solar cells. Renew Energy 2003;28(1):1–12.

[44] Costoya X, deCastro M, Carvalho D, Arguilé-Pérez B, Gómez-Gesteira M. Combining offshore wind and solar photovoltaic energy to stabilize energy supply under climate change scenarios: a case study on the western Iberian Peninsula. Renew Sustain Energy Rev 2022;157:112037.

[45] Wiser RH, Bolinger M, Hoen B, Millstein D, Rand J, Barbose GL, Paulos B. Land-based wind market report: 2021 edition. Berkeley, CA (United States): Lawrence Berkeley National Lab. (LBNL); 2021.

[46] Leon JM, Koivisto MJ, Sørensen P, Magnant P. Power fluctuations in high installation density offshore wind fleets. Wind Energy Sci Discuss 2020:1–23.

[47] Counihan J. Adiabatic atmospheric boundary layers: a review and analysis of data from the period 1880-1972. Atmos Environ 1975;79:871–905.

[48] Hsu SA, Meindl EA, Gilhousen DB. Determining the power-law wind-profile exponent under near-neutral stability conditions at sea. J Appl Meteorol 1994;33:757–65.

[49] Perkins SE, Pitman AJ, Holbrook NJ, McAneney J. Evaluation of the AR4 climate models' simulated daily maximum temperature, minimum temperature, and precipitation over Australia using probability density functions. J Clim 2007;20(17):4356–76.

[50] Ribeiro A, Costoya X, de Castro M, Carvalho D, Dias JM, Rocha A, Gomez-Gesteira M. Assessment of hybrid wind-wave energy resource for the NW coast of iberian Peninsula in a climate change context. Appl Sci 2020;10(21):7395.

[51] Costoya X, deCastro M, Carvalho D, Feng Z, Gómez-Gesteira M. Climate change impacts on the future offshore wind energy resource in China. Renew Energy 2021;175:731–47.

[52] Costoya X, DeCastro M, Carvalho D, Gómez-Gesteira M. On the suitability of offshore wind energy resource in the United States of America for the 21st century. Appl Energy 2020;262:114537.

[53] Haupt SE, Copeland J, Cheng WY, Zhang Y, Ammann C, Sullivan P. A method to assess the wind and solar resource and to quantify interannual variability over the United States under current and projected future climate. J Appl Meteorol Climatol 2016;55(2):345–63.

[54] Gorjian S, Sharon H, Ebadi H, Kant K, Scavo FB, Tina GM. Recent technical advancements, economics and environmental impacts of floating photovoltaic solar energy conversion systems. J Clean Prod 2020:124285.

[55] López M, Rodríguez N, Iglesias G. Combined floating offshore wind and solar PV. J Mar Sci Eng 2020;8(8):576.

[56] Shaner MR, Davis SJ, Lewis NS, Caldeira K. Geophysical constraints on the reliability of solar and wind power in the United States. Energy Environ Sci 2018;11(4):914–25.

[57] Khare V, Nema S, Baredar P. Solar–wind hybrid renewable energy system: a review. Renew Sustain Energy Rev 2016;58:23–33.

[58] Klonari V, Fraile D, Rossi R, Schmela M. Exploring the viability of hybrid wind-solar power plants. In proceedings of the 4th international hybrid power systems workshop, crete, Greece. 2019.

[59] de Doile GND, Rotella Junior P, Rocha LCS, Bolis I, Janda K, Coelho Junior LM. Hybrid wind and solar photovoltaic generation with energy storage systems: a

systematic literature review and contributions to technical and economic regulations. Energies 2021;14(20):6521.

[60] Roy P, He J, Zhao T, Singh Y. Recent advances of wind-solar hybrid renewable energy systems for power generation: a review. IEEE Open Journal of the Industrial Electronics Society 2022.

[61] Le Treut G, Lefevre J, Lallana F, Bravo G. The multi-level economic impacts of deep decarbonization strategies for the energy system. Energy Pol 2021;156:112423.